Zhao *et al. Biochar* (2024) 6:89
https://doi.org/10.1007/s42773-024-00385-4

Biochar

ORIGINAL RESEARCH Open Access

Beryllium adsorption from beryllium mining wastewater with novel porous lotus leaf biochar modified with PO_4^{3-}/NH_4^+ multifunctional groups (MLLB)

Xu Zhao[1], Qingliang Wang[2,4], Yige Sun[3], Haoshuai Li[2], Zhiwu Lei[2], Boyuan Zheng[2], Hongyang Xia[2], Yucheng Su[2], Khan Muhammad Yaruq Ali[2], Hongqiang Wang[2,3] and Fang Hu[2*]

Abstract

Wastewater produced in beryllium mining seriously affects ecological balance and causes great environmental pressure. We designed a novel porous lotus leaf biochar modified with PO_4^{3-}/NH_4^+ multifunctional groups (MLLB) and used it for beryllium(Be) removal from beryllium mining wastewater. Kinetic and thermodynamic experiments showed that the adsorption capacity (Q_e) of Be with MLLB from the simulated beryllium mining wastewater could reach 40.38 g kg^{-1} (35 °C, pH = 5.5), and the adsorption process was spontaneous and endothermic. The dispersion coefficient K_d of Be with MLLB was 2.6×10^4 mL g^{-1}, which proved that MLLB had strong selective adsorption capacity for Be. Phosphoric acid, ammonia, and hydroxyl groups on the MLLB surface would complex with Be to form $Be(OH)_2$ and $Be(NH_4)PO_4$ complexation products, which implied that surface complexation and precipitation reactions might co-existed in the adsorption process. The above results showed that MLLB could effectively adsorb Be and prevent beryllium exposure in a beryllium mining process.

Keywords Biochar, Desorption, Adsorption, Beryllium mining wastewater

*Correspondence:
Fang Hu
csuhufang@163.com
Full list of author information is available at the end of the article

Graphical Abstract

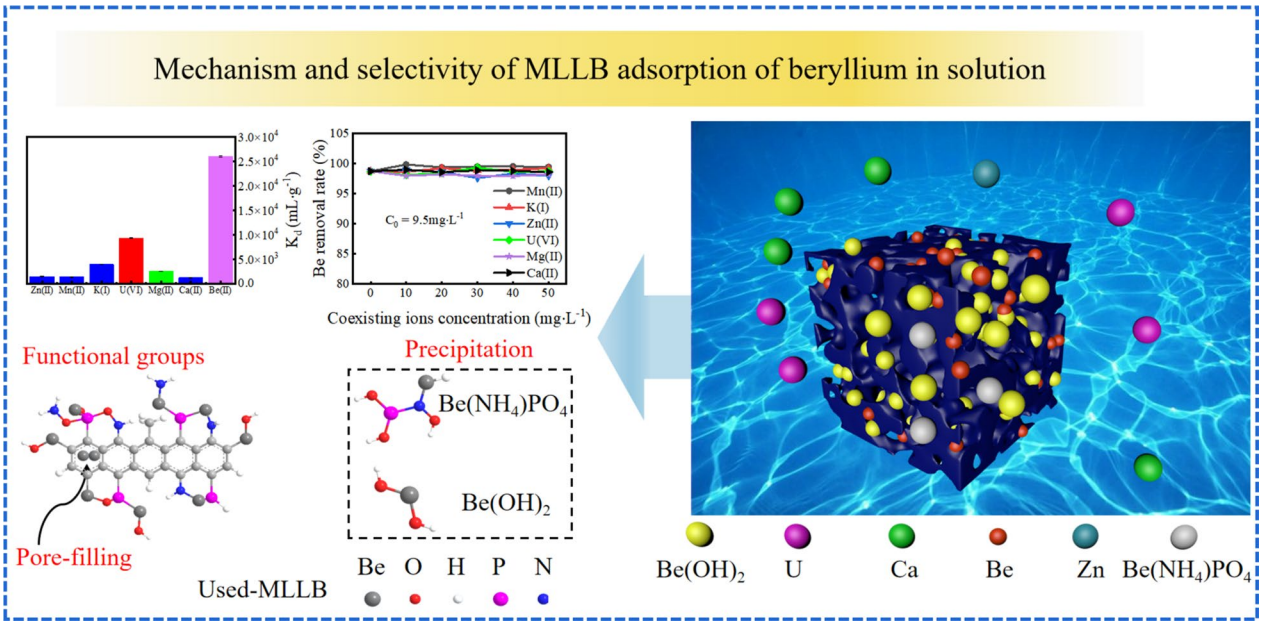

1 Introduction

Beryllium has many excellent properties and is widely used in alloys, aviation and space optics. At present, the occurrence forms of beryllium are hydroxysiloberyllium, greenstone ($3BeO{\cdot}Al_2O_3{\cdot}6SiO_2$), beryllianite ($2BeO{\cdot}SiO_2$), bertrandite $Be_4Si_2O_7(OH)_2$, beryl ($BeO{\cdot}Al_2O_3$) and a few other types. In addition, there are some associated ores such as U–Be ore, Li–Be ore (Lepidolite and spodumene). Currently, only the United States, Kazakhstan and China can process beryllium ores into beryllium products (Lederer et al. 2016). Beryllium occurs in a variety of intermediate materials in the industrial stages of mining, processing, manufacturing and end use. In all aspects of the beryllium industrial chain, beryllium inevitably migrates to groundwater and domestic sewage (Islam et al. 2022). Beryllium is a toxic substance that can cause severe diseases in animals (Creutzenberg et al. 2022) and plants (Tanveer et al. 2019). Long-term exposure to beryllium can damage lungs and other organs. Zhong et al. (2023) evaluated beryllium contamination severity in depth and showed that the leaching beryllium concentration from beryllium-containing sludge was 10,000 times greater than the hazardous waste standard, potentially seriously harming the human living environment. Due to the environmental pressure caused by beryllium, beryllium mining wastewater needs to be treated and beryllium recovered effectively.

Biochar is an excellent adsorbent material with large surface area, porosity, ease of use and convenience (Qu et al. 2023). Biochar has many active groups, but has poor selective adsorption. Tokachkova et al. (2021) concluded that the maximum adsorption capacity of beryllium for biochar modified with Fe_xO_y was only 1.44 g kg^{-1}. The above results show that the adsorption capacity of iron-based biochar is poor. At the same time, only the adsorption effect in a single solution has been studied, and the influence of coexistence ions on the adsorption of biochar to beryllium has not been investigated. Presently, most studies on coexisting ions are conducted in binary systems. For example, Sun et al. (Sun et al. 2011) studied the effects of Cd, Cu and Fe on the beryllium adsorption effect. Studies have shown that activated sludge can still effectively adsorb beryllium in the binary system. Beryllium mining wastewater contains many cations (Zn(II), U(VI), Mg(II), K(I), Ca(II) and Mn(II)) and anions (SO_4^{2-}, NO_3^-, and Cl), which will compete for the adsorbent active site and reduce the treatment effect of existing adsorbent materials. Therefore, in beryllium mining wastewater treatment, how to prepare an efficient and highly selective adsorption material to achieve effective treatment and recovery is a difficult problem.

Because beryllium tends to bind to anions (NH_4^+, PO_4^{3-}, and CO_3^{2-}) mainly through covalent bonds (Bu et al. 1998; Zhao et al. 2023b, 2024), lotus leaf biochar (LLB) was prepared by ammonia leaching and loading

phosphate with lotus leaf as raw material. Lotus is widely planted in China, and its leaves, as agricultural waste, can be used to prepare biochar. Lotus leaf biochar has a high specific surface area, highly active groups and abundant micropores. Prior to this, phosphates were widely used for beryllium determination (De Sousa 1975; Petidier et al. 1985), and showed that phosphate had strong binding ability to beryllium. Besides, soaking lotus leaf biochar in ammonia could destroy its cellulose and other compounds, and the existence of ammonium might lead to dehydration, dehydrogenation or decarbonization reactions (i.e. Maillard reactions) with carbonyl compounds such as aldehydes, ketones, acids and so on. After nitrogen application, the H/C ratio might be effectively increased and O content would be significantly reduced. Studies also have shown that biochar could generate many basic nitrogen-containing functional groups under ammonia impregnation (Zheng et al. 2020). Therefore, we speculate that the introduction of phosphate and ammonium within the biochar might be beneficial for the beryllium adsorption. Our primary objective was to construct and modify the lotus leaf biochar (MLLB) through chemical synthesis and to achieve satisfied Be adsorption effect from beryllium mining wastewater. In this study, we designed and synthesized the novel modified porous lotus leaf biochar(MLLB) and used it to selectively adsorb Be from simulated beryllium mining wastewater. The adsorption thermodynamics and kinetics were studied with different adsorption models, and the adsorption selectivity of Be was evaluated by calculating its distribution coefficient (K_d). Finally, the material's economical and practical values through Be adsorption and desorption were discussed. The adsorption mechanisms were explored via various characterizations. The as-prepared modified porous lotus leaf biochar seems to be a new, effective and inexpensive adsorption material for relieving the environmental pressure caused by beryllium mining wastewater.

2 Material and methods

2.1 Materials

BeO (purity: ~ 98%, CAS Number: 1304-56-9), $Ca(OH)_2$ (purity: ~ 95%, CAS Number:1305-62-0), H_3PO_4 (purity: ~ 89%, CAS Number: 7664-38-2, AR), $FeSO_4{\cdot}7H_2O$ (purity: ~ 99%, CAS Number: 7782-63-0), $Zn(NO_3)_2{\cdot}6H_2O$ (purity: ~ 98%, AR), KCl (purity: ~ 99%, CAS Number: 7447-40-7), and $MnSO_4$ (purity: ~ 99%, CAS Number: 7785-87-7) were purchased from Sinopharm Chemical Reagent Co., Ltd.

2.2 MLLB preparation method

The lotus leaves used in the experiment were picked when fully open and blade diameter was 25–50 cm. Lotus leaves were dried and crushed through a 30 or 40-mesh sieve, and 50 g of lotus leaf powder was immersed in 100 mL 5% diluted ammonia water. Then, the powder was extracted and pretreated at 105 °C for 12 h. According to the molar ratio of $Ca(OH)_2$: H_3PO_4 = 3: 3, a certain mass of calcium hydroxide and phosphoric acid was weighed, and mixed with the pre-treated lotus leaf powder in a beaker. Water, at a mass ratio of 1:2, as well as phosphoric acid, was added by drip at 600 r min^{-1} for 1 h. The mixture was oven-dried at 120 °C until it did not flow. The dried mixture was ground after roasting at 600 °C in a Muffle furnace for 3 h and then sifted through 80 mesh to obtain MLLB (Fig. 1).

2.3 Preparation of simulated wastewater from beryllium mining

According to Wang et al. (2019), beryllium ore contains various elements, such as Zn(II), Be(II), U(VI), Mg(II), K(I), Ca(II) and, Mn(II). In this experiment, a solution containing Zn, Mn, Ca, Mg, U, and K (10–50) mg L^{-1} was prepared to simulate beryllium mine mining wastewater (pH = 5.5). The concentrations of the above elements were measured by ICP-MS (Agilent, Agilent 720ES). The dispersion coefficient K_d was calculated using Eq. (1) (Xin et al. 2023).

$$K_{\mathrm{d}} = \frac{(C_0 - C_e) \times V}{C_e \times m} \times 1000 \tag{1}$$

where C_0 (mg L^{-1}) is the initial beryllium concentration, C_e (mg L^{-1}) is the beryllium concentration at adsorption equilibrium, V is the Be solution (mL) volume and m is the MLLB dosage (g).

2.4 Batch experimental analysis

We designed a batch experiment, with initial pH, amount of adsorbent and the adsorption of simulated wastewater from beryllium mining. The kinetic and thermodynamic results of adsorbed materials were analyzed in a quasi-combined manner. In principle, it is not necessary to change the mining wastewater temperature, and the temperature detected in this experiment was only to prove that MLLB has a strong beryllium adsorption capacity within the temperature range studied. Initial pH was measured to demonstrate the MLLB adsorption mechanism to beryllium and to determine that MLLB can effectively remove beryllium from the beryllium mining wastewater acid-base environment.

Three sets of parallel samples were used in batch experiments to confirm the accuracy of the results. The first batch experiment was conducted to study the effect of W_{CP}:W_{LLB} (wt:wt) = 1:10, 1:2, 1:1, 2:1, 5:1 on the adsorption effect. For five different materials, 0.05 g of each was placed in a 50 mL solution to form a mixed liquid, and

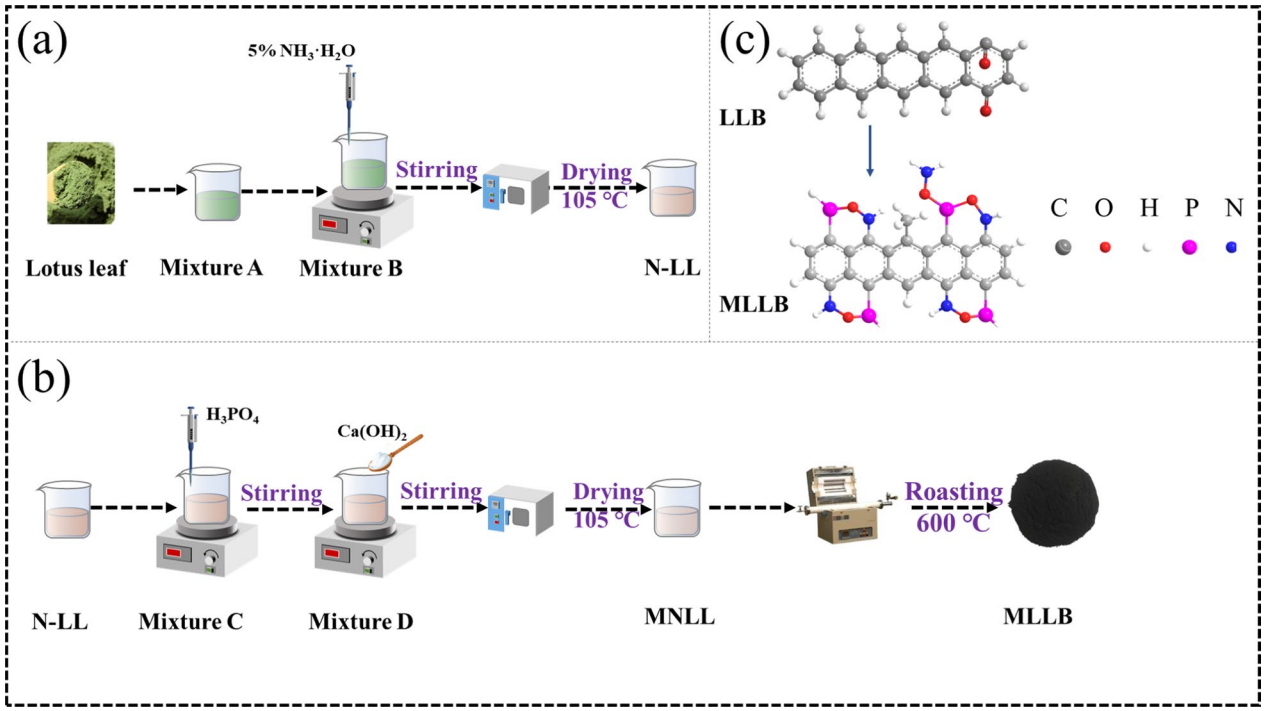

Fig. 1 Preparation of MLLB

the mixture was placed in a shaking table under reaction conditions of 25 °C, 175 r min^{-1} and 16 h. The mixture was separated and beryllium concentration in the clarified solution was measured with a UV–Visible spectrophotometer (Eqs. 2–4).

$$C = \frac{(A - 0.0038)}{0.2} \tag{2}$$

$$q_e = \frac{V(C_0 - C_e)}{m} \tag{3}$$

$$R = \frac{C_0 - C_e}{C_0} \times 100\% \tag{4}$$

where A is the absorbance, C (mg L^{-1}) is the beryllium concentration, C_0 (mg L^{-1}) is the initial beryllium concentration, C_e (mg L^{-1}) is the beryllium concentration at adsorption equilibrium, V (L) is the Be solution volume, and m is the MLLB dosage (g).

2.5 Desorption

In this study, 3 M HCl, 3 M H_2SO_4, 10% $NaCO_3$ and 10% NaOH solution were used to perform desorption tests in a constant temperature oscillation chamber at a rotating speed of 175 r min^{-1}. The experimental temperature was 25 °C, and 0.1 g Used-MLLB was added into 25 mL desorption solution for 2 h. After the reaction, the mixed solution was separated, the solid was placed in the oven to dry, and the liquid was used for measurement. The dried solid was adsorbed–desorbed five times according to the above steps. The amount of desorption ion (q_ed_e) was calculated by the following equation (Zhao et al. 2023a):

$$q_e d_e = \frac{(C_e d_e)V}{W} \tag{5}$$

where C_ed_e is the metal concentration in the solution after the desorption step, V is the solution volume (L), W is the solid mass (g), and the percentage of desorption beryllium (DE) is calculated as:

$$DE(\%) = \frac{(q_e d_e)100}{q_e a_d} \tag{6}$$

Among them, q_ea_d and q_ed_e are adsorbent adsorption and desorption amounts, respectively.

2.6 Characterization method

The MLLB surface elemental composition was analyzed using XPS (Thermo Fisher Scientfc KAlpha instrument). For calibration, the spectrum binding energy was normalized by the C 1 s peak at 284.8 eV. XRD was measured by D8 advanced x-ray diffractometer, and MLLB material composition and Used-MLLB were mainly analyzed. A TG thermogravimetric analyzer (TG/DTA7300)

instrument was used to analyze the MLLB and Used-MLLB. Different absorption heat peaks and sample weight losses identified content of different substances in the sample. MLLB specific surface and porosity were measured by BET (3H-2000BET-A), and FTIR was used to measure MLLB and Used-MLLB group types. Surface morphology of MLLB and Used-MLLB was measured by SEM, and the element composition of MLLB and Used-MLLB was measured by EDS. Zeta potential was measured by Malvern Zetasizer Nano ZS.

3 Results and discussion

3.1 Characterization

To further explore the synergism between phosphoric acid and ammonia in the adsorption process, we prepared four different biochar types: biochar without phosphoric acid and ammonia (LLB); biochar with only ammonia (NLLB); biochar with only phosphate (PLLB); and biochar with phosphoric acid and ammonia (NPLLB) (Additional file 1: Fig. S1a, b). Comparing the above four biochar types and MLLB biochar, we found that the effect of adding phosphate was the worst because its adsorption effect was poor at low pH (Zhao et al. 2023a). Compared to PLLB, LLB and NLLB had stronger adsorption capacity, mainly due to increased functional groups from ammonia immersion. After ammonia impregnation and pyrolysis, the carbonyl compounds in biochar can be converted to N heterocyclic compounds, and solid biochar specific surface area, total nitrogen content and number of nitrogen-containing functional groups also significantly increase (Zheng et al. 2020). The adsorption efficiency of some biochar for beryllium is MLLB > NPLLB > NLLB > LLB > PLLB, mainly because beryllium exists in solution as a cation, and the addition of ammonia reduces the biochar surface charge, resulting in electrostatic attraction. The addition of phosphoric acid will increase the biochar surface charge, which will generate electrostatic repulsion. The simultaneous addition of phosphoric acid and ammonia will form stable complexes with beryllium, and the adsorption effect of biochar will improve. The NPLLB adsorption effect was lower than MLLB, mainly because the added calcium hydroxide neutralizes the phosphoric acid hydrogen ions, and part of the phosphate supported on the biochar surface is in the form of calcium phosphate, so that more phosphate can be dissolved during the adsorption process. These results show that it is feasible to adsorb beryllium on biochar with phosphate and amino groups.

Biochar surface morphology before and after modification was characterized with a scanning electron microscope (SEM). The LLB surface had fewer pores and a relatively flat surface, while MLLB was irregularly shaped, with many pores of different sizes providing a large specific surface area (Fig. 2a–f). MLLB is a compound biochar prepared by covering the lotus leaf surfaces with phosphoric acid and ammonia base groups. During the adsorption process, MLLB pores play an adsorption role (Zhao et al. 2023a). There was more P on MLLB, indicating that the phosphate groups are well fixed on the biochar as supported in the energy dispersive spectrum (EDS) LLB and MLLB diagrams (Fig. 3a, b).

Brunauer, Emmett, and Teller (BET) was used to analyse the different modifications to biochar porosity, pore size and specific surface area between LLB and MLLB. The LLB specific surface area was 4.927 $m^2\ g^{-1}$, and the pore size was 3.864 nm, showing a mesopore morphology (Fig. 3c). LLB and MLLB have a type III adsorption isotherm (Zhao et al. 2023c; Thommes et al. 2015). The MLLB specific surface area was 16.674 $m^2\ g^{-1}$, and the pore size was 3.820 nm, showing a mesopore shape (Fig. 3d). Due to a load of phosphate groups and ammonia root groups, Ca^{2+} and phosphate groups are

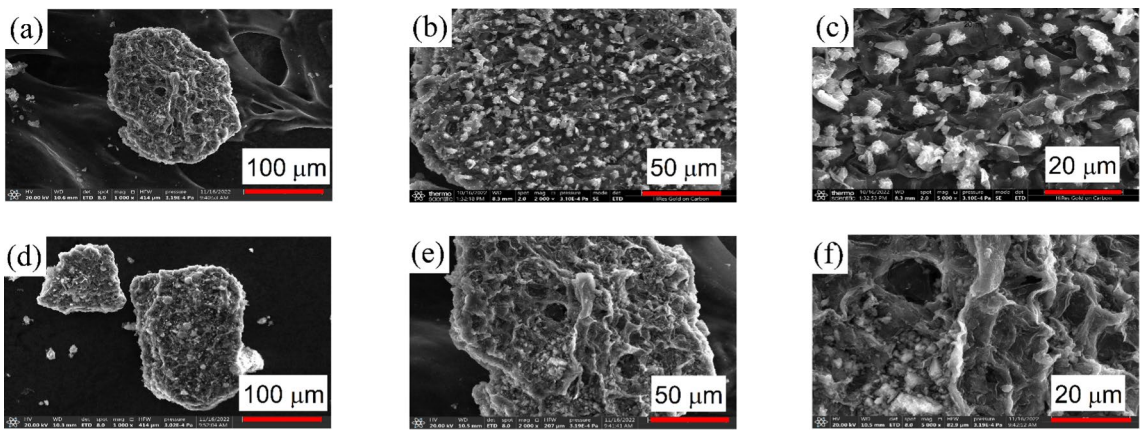

Fig. 2 SEM of LLB (**a**–**c**) and MLLB (**d**–**f**)

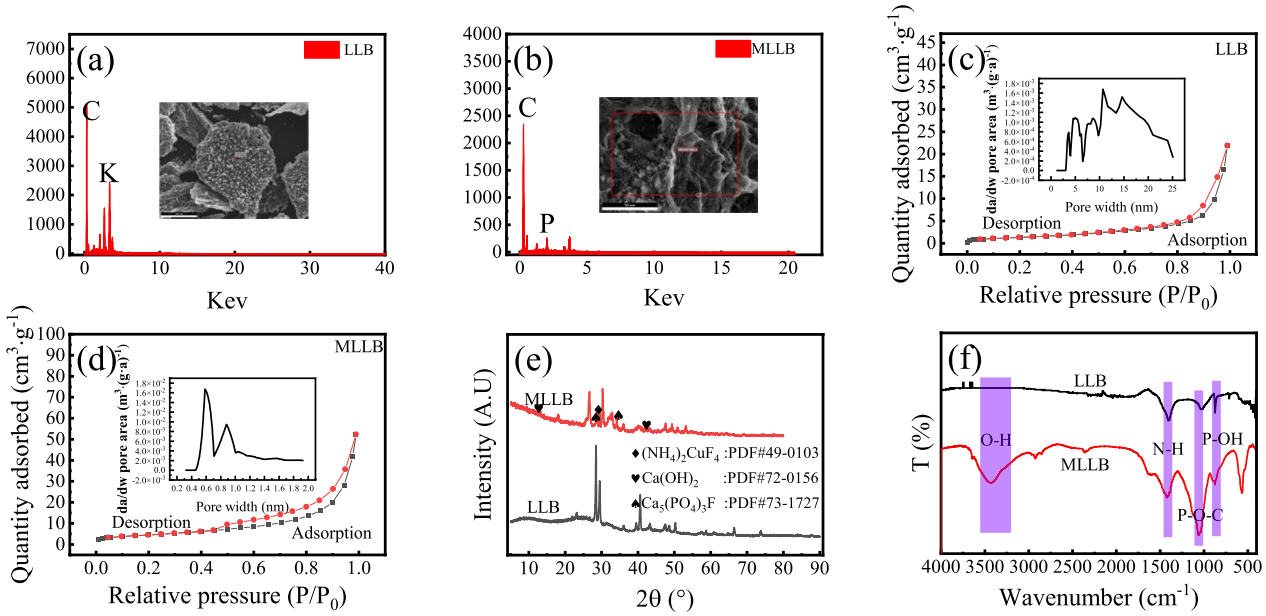

Fig. 3 EDS analysis of LLB (**a**) and MLLB (**b**), BET analysis of LLB (**c**) and MLLB (**d**), XRD pattern of LLB and MLLB (**e**), FT-IR pattern of LLB and MLLB (**f**)

embedded in the MLLB pore structure or cross-linked on the MLLB surface, and the network void structure cannot be filled entirely, thus increasing the MLLB specific surface area.

X-ray diffraction (XRD) was used to analyze material changes on the LLB and MLLB surfaces, and LLB and MLLB crystalline phases (Fig. 3e). For LLB, wide amorphous carbon peaks at 20–25° were detected, indicating the formation of aromatic carbon skeleton structures (Wei et al. 2022); however, they weakened on MLLB. $CaCO_3$ (PDF#05-0586) diffraction at $2\theta = 29.6°$ on MLLB was clearer than on LLB. Additionally, for MLLB we found typical $Ca(OH)_2$ (PDF#72-0156) peaks near 2θ at 19.8° and 52.3°, and typical $Ca_5(PO_4)_3$ (PDF#73-1727) at 37.2° and 39.4°. A typical $(NH_4)_2CuF_4$ (PDF#49-0103) peak was found at 31.2°. These results indicate that phosphate and ammonia base groups are well supported on the MLLB surface.

Fourier Transform infrared spectroscopy (FT-IR) was used to explore changes in biochar functional groups before and after modification (Fig. 3f). Peaks extending to 3550–3100 cm^{-1} and 1400 cm^{-1} corresponded to the –OH and N–H groups, respectively (Wei et al 2022; Qu et al. 2024). They were more sensitive to MLLB than to LLB. Meanwhile, stretching bands at 1150, 810, and 520 cm^{-1} corresponded to the vibrations of P–O–C, P–OH and inorganic MLLB content, respectively (Xin et al. 2023) and vibrations of the above peaks were enhanced for MLLB. This difference is due to changes in biochar structure during group loading. The above results indicate the success of MLLB preparation.

3.2 Batch experiment

To explore the optimal MLLB preparation conditions, it was prepared according to different proportions of species and its adsorption effect was discussed. The W_{CP}:W_{LLB} ratio was positively correlated with adsorption efficiency, and the Q_e (9.45 g kg^{-1}) was reached when W_{CP}:W_{LLB} reached 2:1 (Fig. 4a). When W_{CP}:W_{LLB} (wt:wt) < 2:1, there are more functional groups on the biochar surface because there is more phosphoric acid and calcium hydroxide, thus improving MLLB adsorption efficiency. When W_{CP}:W_{LLB} (wt:wt) > 2:1, pore size of the material may be reduced to a certain extent under the reduction of biochar, thus reducing the surface adsorption effect. Therefore, W_{CP}:W_{LLB} was used as 2:1 to prepare the sample. Adsorbent dosage involves economic practicality, and MLLB removal efficiency is positively correlated with the amount of adsorbent. Maximum adsorption efficiency reached 98% when MLLB was 2 g L^{-1} (Fig. 4b), therefore, the dosage of all adsorbents in this experiment was 2 g L^{-1}.

Solution pH will impact the chemical form of beryllium. When pH is < 5.5, beryllium exists as a free ion, but when pH is > 5.5, $Be(OH)_2$ precipitates and exists as a complex form of $Be_2(OH)_2^{2+}$ (Mahmoud et al. 2018). Optimal MLLB adsorption efficiency was 99% when pH was 5–7 (Fig. 4c). To establish a suitable adsorption

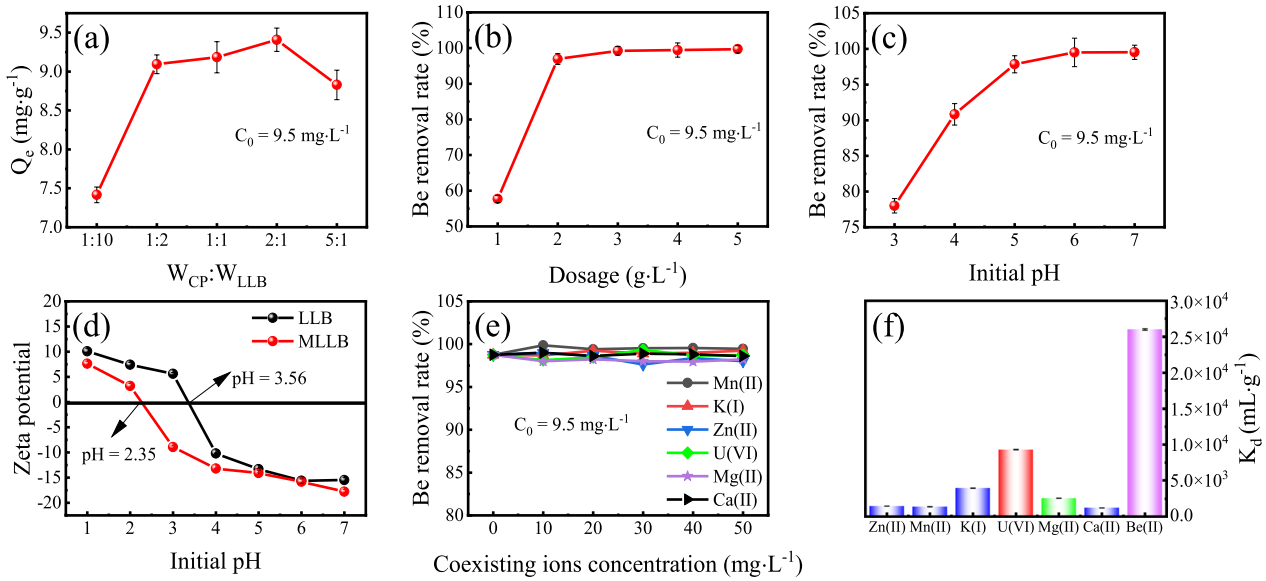

Fig. 4 Sample preparation (**a**), effect of adsorbent dosage (**b**), influence of initial pH (**c**), Zeta potential of LLB and MLLB (**d**), influence of competing ions on removal (**e**), K_d of competing ions in mixed solution (**f**)

mechanism, Zeta potential analysis was carried out for samples under different equilibrium pH values. MLLB and LLB zero point charges were located at pH = 2.35 and pH = 3.56, respectively (Fig. 4d). Compared with LLB, MLLB had a more substantial negative surface charge, which was positively correlated with pH. Since the beryllium complex has a positive charge in the measured pH range, it generates electrostatic attraction with the negative charge on the material surface (Zhao et al. 2023a), thus holding the beryllium to the material surface. Mining is becoming more environmentally friendly. Therefore, most of the mining wastewater is in the pH range of 5–8 (Fan et al. 2024), and the adsorbent can treat the mining wastewater well.

Considering that many ions co-exist in industrial beryllium-containing wastewater, such as cations like Zn, Mn, U, Mg, Ca and K, as well as anions such as SO_4^{2-}, Cl^-, and NO_3^-, we investigated the influence of competing elements on beryllium adsorption rate. Five cations, Zn, Mn, U, Mg, Ca and K, were considered as the interfering ions and the concentration gradient was 10, 20, 30, 40, and 50 mg L^{-1}. Since beryllium in solution exists in the form of cations when pH is less than 10, the influence of anions is not considered. MLLB beryllium removal efficiency in several binary systems (Be–Zn, Be–Mn, Be–U, Be–Mg, Be–Ca and, Be–K) ranged from 97 to 99% (Fig. 4e). So in the binary system, Zn, Mn, U, Mg, Ca and K for MLLB had little effect on beryllium adsorption. The K_d of Be (II) on MLLB was 2.6×10^4 mL g^{-1}, which was much higher than Zn(II) ($K_d = 1.45\times10^3$ mL g^{-1}), Mn(II) ($K_d = 1.36\times10^3$ mL g^{-1}), Ca(II) ($K_d = 1.20\times10^3$ mL g^{-1}), Mg(II) ($K_d = 2.56\times10^3$ mL g^{-1}), K(I) ($K_d = 3.95\times10^3$ mL g^{-1}), and U(VI) ($K_d = 9.3\times10^3$ mL g^{-1}), indicating that MLLB still had an excellent selective adsorption capacity for beryllium in the presence of interfering ions (Fig. 4f). The high U(VI) K_d may be due to the adsorption effect of phosphate groups on uranium (Xin et al. 2023).

3.3 Adsorption kinetics

Beryllium adsorption kinetic behavior on MLLB was investigated with three kinetic models, and the relationships between time, temperature, and adsorption capacity were established. The longest adsorption time to prevent MLLB desorption (Shchukarev et al. 2004) was 16 h. Most adsorbates were rapidly adsorbed in the early phase (Fig. 5a–c), and removal equilibrium was achieved within 2 h of adsorption, with a maximum adsorption efficiency of 99%. A comparison of the R^2 ($R_F^2 = 0.99325$, $R_S^2 = 0.99849$, $R_I^2 = 0.9422$) of the three different adsorption kinetics showed that they well fit the removal process at 35 °C and proves that it is mainly chemical adsorption, such as ion exchange and surface complexation (Zhang et al. 2021), while physical adsorption and in-case diffusion exist simultaneously (Table 1). The fitting of the in-sample diffusion model was divided into three line segments (Fig. 5c; Wu et al. 2005). The R^2 of the first and second stages approached 0, which proves that the rate-limiting process in the removal reaction is liquid film diffusion (Liu et al. 2010).

3.4 Adsorption isotherm

For the three thermodynamic models used, the Langmuir model considers the effect of temperature and can effectively predict maximum adsorption concentration (Fig. 5d–f). The Langmuir model applies to the reaction process, and the fitting coefficient $R^2 = 0.934$ indicates that the solid and liquid reaction is mainly chemical (Table 2) (Bonilla–Petriciolet et al. 2017). Furthermore, the adsorbent is uniformly fixed on the MLLB surface. The fitted MLLB maximum Q_e was 38.44 g kg^{-1}, and the actual Q_e was 40.38 g kg^{-1} (Fig. 5d–f). Freundlich's fitting coefficient $R^2 = 0.970$, which proves that it also predicts the reaction process well (Pezoti et al. 2016). Freundlich's relevant data showed that $1/n_F$ was between 0.1 and 0.5, indicating that beryllium is quickly adsorbed by MLLB (Mirzaeei et al. 2019). Temkin's fitting coefficient $R^2 = 0.974$ indicates that the Temkin model can also be used to fit the reaction between MLLB/beryllium, suggesting that the binding energy in the MLLB adsorption process is uniformly distributed (Guerrero–Fajardo et al. 2020). About 80% of adsorbents had adsorption capacities below 40 g kg^{-1} (Additional file 1: Table S1).

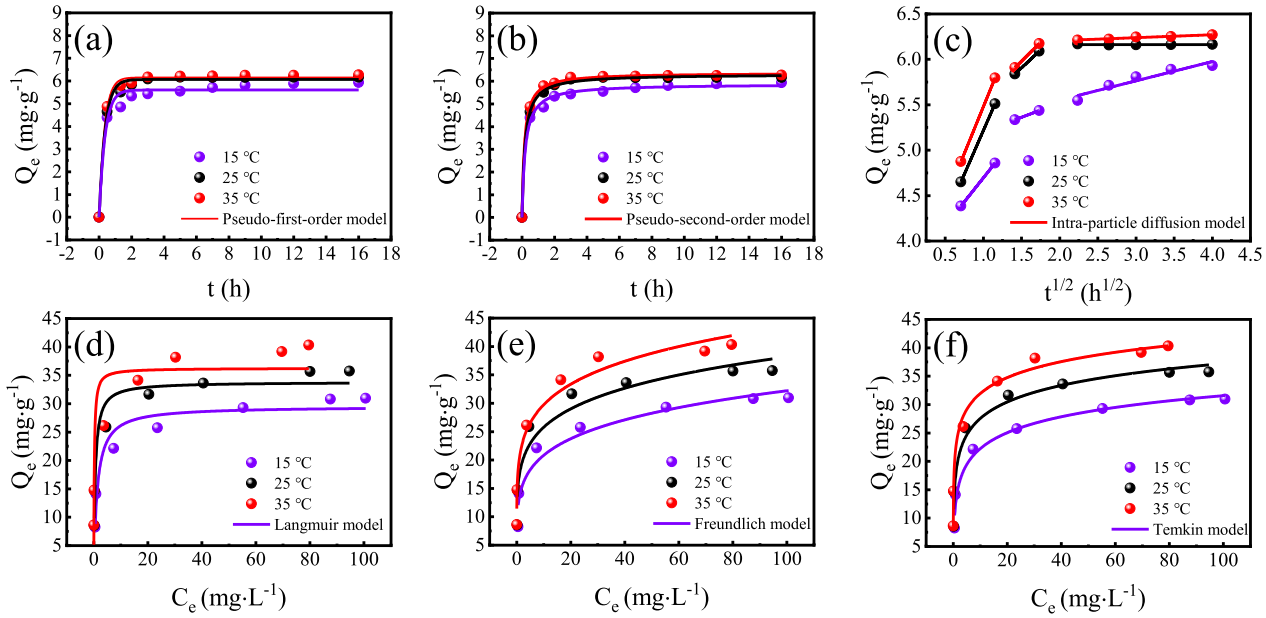

Fig. 5 Adsorption kinetics fitting (**a**–**c**), Adsorption thermodynamic fitting (**d**–**f**)

Table 1 Parameters of kinetic models for the adsorption of Be(II) onto MLLB

T	Pseudo-first order			Pseudo-second order				Intraparticle diffusion model			
	q_e	k_1	R^2	*RMSE*	q_e	k_2	R^2	*RMSE*	k_s	*C*	R^2
15 ℃	5.422	2.563	0.96888	0.07266	5.693	0.873	0.99222	0.01723	1.132	3.72	0.9890
25 ℃	6.100	2.632	0.99229	0.04338	6.227	0.899	0.99693	0.00395	1.522	3.66	0.9310
35 ℃	6.135	3.128	0.99325	0.03118	6.352	1.100	0.99849	0.00301	2.135	3.91	0.9422

Table 2 Parameters of isotherm models for the adsorption of Be(II) onto MLLB

T (°C)	Langmuir			Freundlich			Temkin		
	K_L	Q_m	R^2	K_F	$1/n_F$	R^2	a_t	b_t	R^2
15	0.769	30.62	0.934	13.45	0.189	0.934	23.93	0.590	0.974
25	1.811	34.81	0.932	17.40	0.170	0.917	69.57	0.589	0.967
35	5.357	38.44	0.856	20.33	0.165	0.970	260.99	0.631	0.851

By comparison, the actual MLLB adsorption capacity was 40.38 g kg^{-1}, which is better than most current adsorbents.

3.5 Thermodynamics

Thermodynamics can effectively express energy change in the adsorption process. We calculated thermodynamic parameters by fitting thermodynamic formulae (Equation S8–S11). $\Delta G^0 = -26.84$ kJ $mol^{-1} < 0$ indicates that beryllium is more readily adsorbed by MLLB, and the MLLB/beryllium adsorption process is spontaneous (Additional file 1: Table S2) (Ren et al. 2021). $\Delta H^0 = 2.29$ kJ $mol^{-1} > 0$ indicates that the removal process is a thermonegative response. The absolute value of ΔH^0 increased with increased temperature, which can be explained by the fact that temperature promotes the chemical reaction on MLLB (Liu et al. 2008). $\Delta S^0 = 35.95$ J $(mol\ K)^{-1} > 0$ shows that the energy at the solid-liquid interface increases disorder during the removal process (Basargin et al. 2012).

3.6 Desorption and recycling

As mentioned above, MLLB cycle usage was tested using an adsorption–desorption cycle (Fig. 6a–c). In the cyclic experiment, the beryllium-containing solution concentration was 1 mg L^{-1}, and 3 M HCl, 3 M H_2SO_4, 10% $NaCO_3$ and 10% NaOH solutions were used as desorption agents, and the analytical time was 2 h (Zhao et al. 2023b). In the first desorption process, HCl and H_2SO_4 desorption efficiency were > 90%, and NaOH and $NaCO_3$ desorption efficiency were > 80% (Fig. 6a). In the second MLLB, adsorption efficiency after acid desorption was < 20%, and the second MLLB adsorption efficiency after alkali desorption was > 90%. Therefore, 10% NaOH was selected as the eluent. MLLB adsorption efficiency was 99% in the first cycle and then decreased to 82% in five cycles (Fig. 6b–c), perhaps because pores on the object's surface were occupied by adsorbates, and the surface functional groups were lost in adsorption–desorption. The first desorption efficiency was 90%, and the desorption efficiency was stable at 90% in the following five cycles. Furthermore, MLLB can effectively adsorb beryllium solution in five-cycle experiments, which proves that it can be effectively recycled and reduce cost.

3.7 Carbon footprint

The biochar produced by slow pyrolysis in this study is similar to that described by Desjardins et al. (2024), who simulated the use of wood chips from forests as pyrolysis feedstock. In short, after drying the harvested debris to 7% moisture content, it was put into the pyrolysis reactor at 450 °C for about 42 min. The yield was 29.0% biochar, 40.8% bio-oil and 30.2% biogas. The bio-oil and biogas produced during the pyrolysis process are burned in the burner, producing the heat required for pyrolysis (including the pre-drying step) as well as waste heat. The emission from the pyrolysis stage is 0.015 $tCO_{2eq}\ t_{biochar}^{-1}$–0.052 $tCO_{2eq}\ t_{biochar}^{-1}$. If the bio-oil and biogas produced during the pyrolysis process are not used for power generation/heating, the production emissions are 0.178–0.211 $tCO_{2eq}\ t_{biochar}^{-1}$. (Puettmann et al. 2020).

3.8 Adsorption mechanism

SEM can effectively analyze the morphology of the sample surface and provide effective evidence for the adsorption mechanism. The MLLB surface had a larger pore structure, which was irregular (Fig. 7a–c). SEM images of Used-MLLB are shown in Fig. 7d–f. The adsorbed material surface had flocculents, and the surface pores were filled with floc, which proves that more precipitates occurred on the surface (Fig. 7). The MLLB EDS analysis diagram is shown in (Fig. 8a, b). O and P elements increased significantly after adsorption (Fig. 8).

Used-MLLB and MLLB phases were analyzed by XRD. There were more calcium phosphate and calcium hydroxide on MLLB, indicating that ammonia and phosphoric acid were successfully introduced into the material during the modification process (Fig. 8c). A $Be(NH_4)$

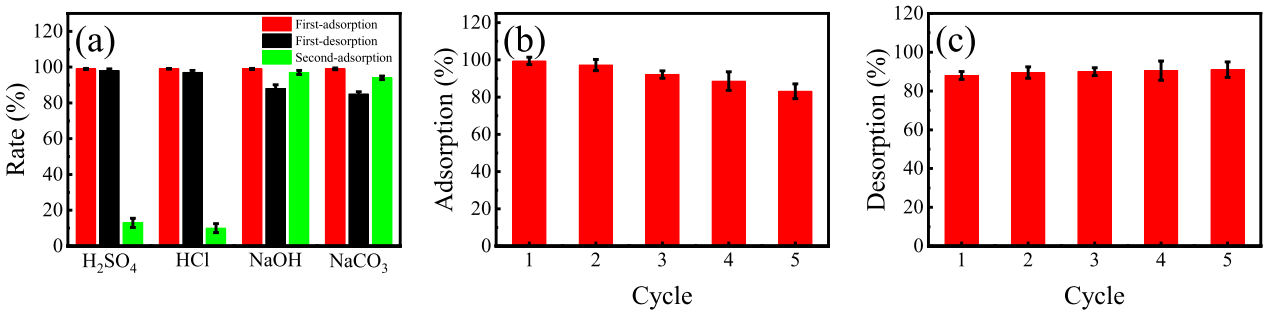

Fig. 6 Influence of different eluents on desorption effect (**a**), cyclic adsorption (**b**) and desorption (**c**)

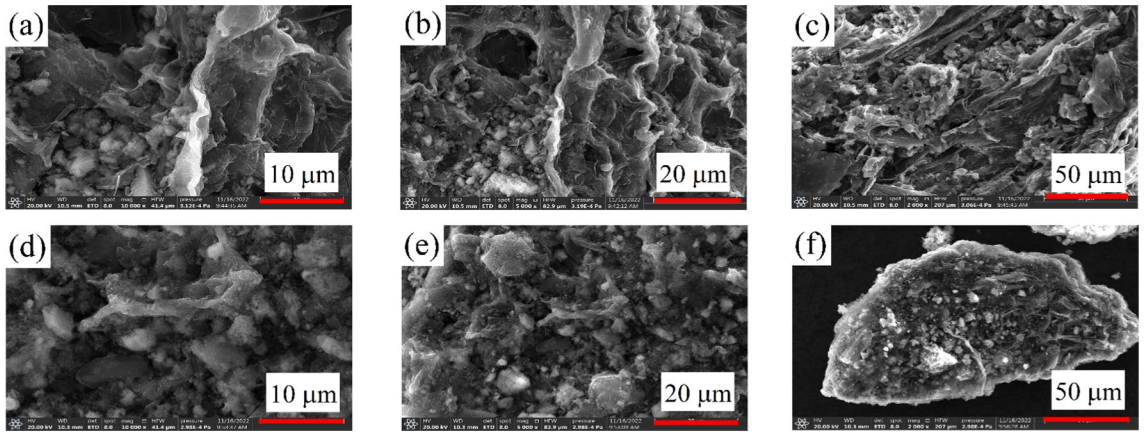

Fig. 7 Scanning electron images (SEM) of MLLB (**a**–**c**) and Used-MLLB (**d**–**f**)

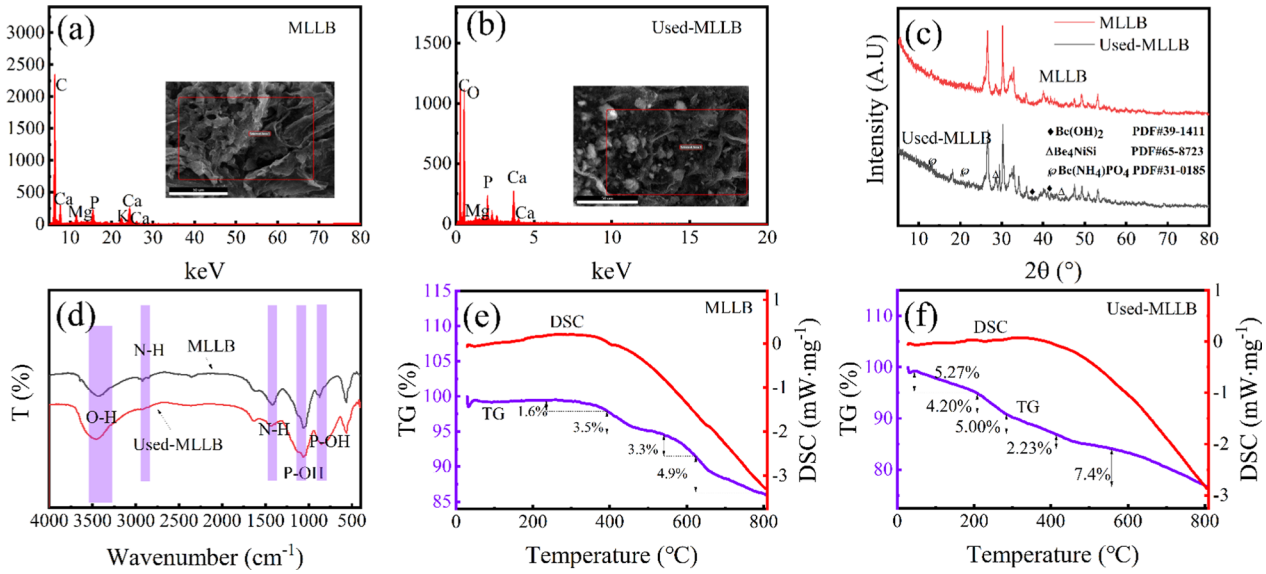

Fig. 8 Energy dispersive spectrometer (EDS) analysis of MLLB (**a**) and Used-MLLB (**b**). XRD analysis (**c**), FT-IR analysis (**d**), Thermal Gravimetric Analyzer (TG) analysis of MLLB (**e**) and Used-MLLB (**f**)

PO_4 (PDF#31-0185) peak was generated at 2θ = 13.5° and 18.9°. Standard $Be(OH)_2$ (PDF#39-1411) peaks were generated at 2θ = 37.5° and 42.3°, and a Be_4SiNi (PDF#65-8723) peak was generated at 2θ = 29.8°. When beryllium ion pH is neutral, it will precipitate with phosphoric acid and ammonia, and there is ammonia-beryllium phosphate in the product (Krishnamoorthy et al. 1969; Al Isawi et al. 2022). These results show that beryllium is effectively fixed on the MLLB surface, and the chemical reaction during adsorption is mainly chelation.

During the removal process, the change of functional groups is the most important reaction index. We used FT-IR to analyze the functional groups on MLLB and Used-MLLB. Vibration of the O–H root was represented at 3500 cm^{-1} (Fig. 8d) (Martins et al. 2015), and N–H vibration at 2700 cm^{-1} and 1475 cm^{-1} (Polowczyk et al. 2016). Vibration at 1135 cm^{-1} represents the in-plane bending band of P–O–H (P. Senthil et al. 2011), and vibration at 859 cm^{-1} represents P–O stretching in PO_4^{3-} and HPO_4^{2-} (Touny et al. 2018; Xin et al. 2023). The FT–IR comparison before and after adsorption showed enhanced the O–H and P–O bonds at 3500 cm^{-1} and 859 cm^{-1}, while the bands at 2700 cm^{-1}, 1475 cm^{-1}, and 1135 cm^{-1} were weakened. Combined with XRD, the oxides gathered on the substance surface after adsorption, proving that $Be(OH)_2$ and $Be(NH_4)PO_4$ precipitates were generated during the experiment.

Notably, beryllium has a strong affinity for N−H, O−H, and PO_4^{3-} groups.

According to the mass loss characteristics of different substances at different temperatures, thermogravimetric analysis (TG) was used to analyze substance content on MLLB and Used-MLLB. Multiple endothermic peaks were observed on MLLB (Fig. 8e). The first peak occurred at 285 °C, possibly due to the disappearance of the water in $CaHPO_4$ (Laohavisuti et al. 2021). The last peak occurred at 675 °C, corresponding to MLLB dehydroxylation characteristics (Jamil et al. 2019). There were also multiple peaks on Used-MLLB (Fig. 8f), the mass loss of the first peak was 3.08%, and the minimum was about 79 °C due to the removal of adsorbed and interlayer water (Sternik et al. 2017). There was a peak around 200 °C, corresponding to the removal of ammonia roots from ammo beryllium phosphate, followed by a substantial mass loss at 280−675 °C, mainly due to the condensation of hydrogen phosphate ions into pyrophosphate ions prior to the decomposition of calcium phosphate (Jamil et al. 2019). The final peak mass loss of Used-MLLB was 5.37% higher than that of MLLB, corresponding to the removal of hydroxyl groups (Jamil et al. 2019), mainly due to the formation of $Be(OH)_2$ precipitate during the reaction. During the adsorption process, beryllium was complexed by hydroxyl group in solution to form a precipitate and attached to the biochar surface, resulting in an increase of hydroxyl group after adsorption. At the same time, some MLLB substances were dissolved into the solution, resulting in an increase in the mass ratio of hydroxyl groups.

X-ray photoelectron spectroscopy (XPS) analysis can be very effective in determining changes in element valence state in substances from the change of material form. The change of material form in the reaction process is illustrated by adsorption increases or decreases in the peak value of various elements (Fig. 9; Labgairi et al. 2020). After the reaction, two peaks were generated at 286.5 and 288.6 eV, which are considered C−OH & C−O−P, and O−C=O & O−C−O, respectively (Fig. 9b, c).

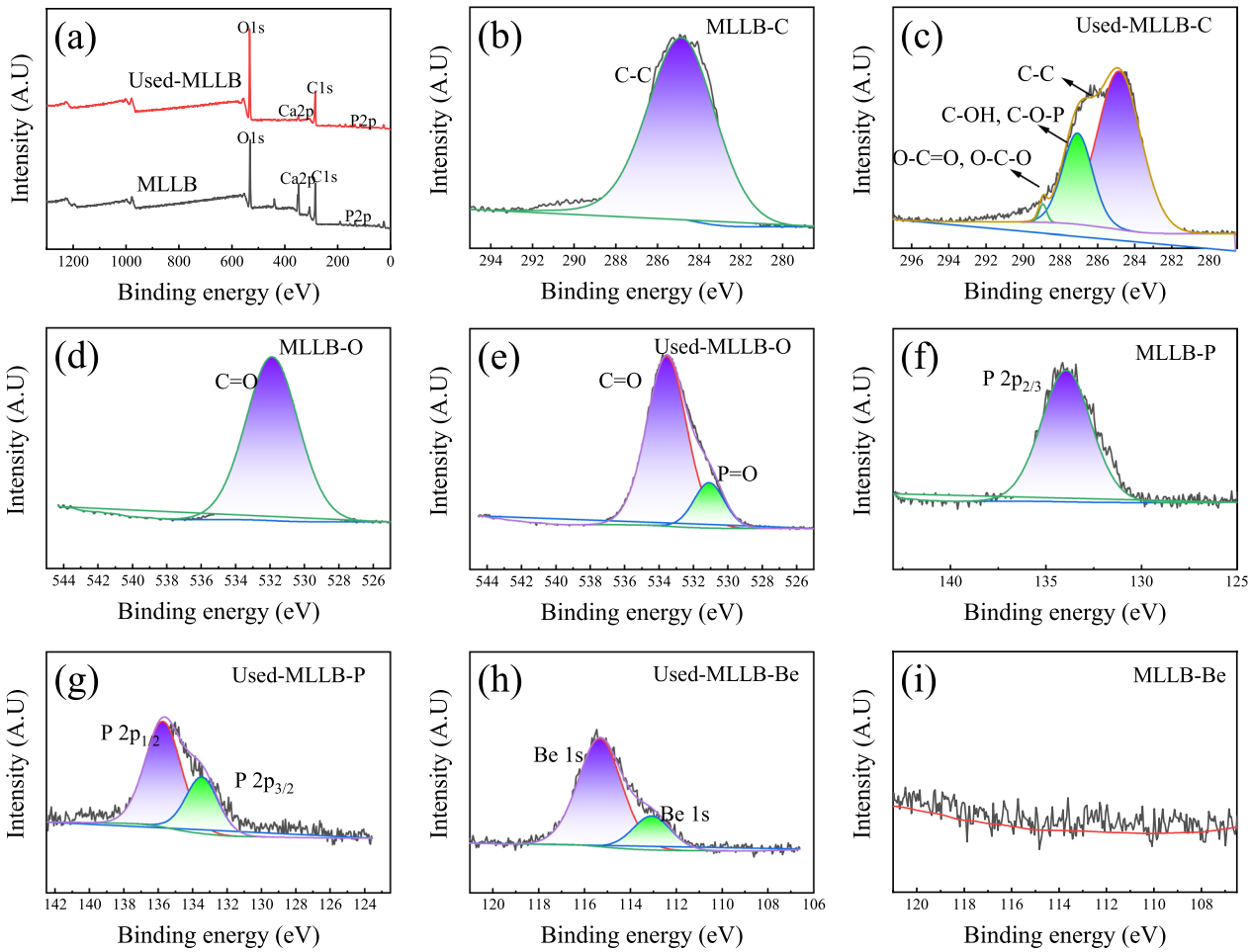

Fig. 9 XPS analysis of MLLB and Used-MLLB

The C=O bond shifted to the left and generated a new metal oxide peak value, proving the energy change and a new peak was generated at 531 eV, which was thought to be P=O (Fig. 9d, e). Phosphorus energy changed from 133 to 135 eV, indicating that phosphorus produces energy changes and participates in the reaction process (Fig. 9f, g). A $P2p_{3/2}$ peak was generated at 133.2 eV, which is generally thought to be a phosphoric acid group complexing with beryllium to form a new substance (Xin et al. 2023). Considerable beryllium existed on Used-MLLB, mainly in beryllium-copper complexes (Fig. 9h, i). Similar to XRD, EDS, and FT-IR results, XPS spectrogram analysis showed that phosphoric acid was involved in the reaction process, proving ammonia-beryllium phosphate precipitation.

According to physicochemical properties analysis, adsorption kinetics, and beryllium/MLLB adsorption system thermodynamic data, there are various physicochemical reactions in the removal progress. MLLB is a porous material. From kinetic data fitting, we found that chemical adsorption is the primary process, physical adsorption exists simultaneously, and adsorption rate is affected by the internal diffusion model. Based on FT-IR, XRD, XPS, and SEM, we successfully fabricated MLLB, which had significant phosphoric acid and ammonia. In the removal progress, MLLB adsorption sites were initially occupied, and then free phosphoric acid, ammonia, and hydroxyl groups were complexed by beryllium. TG analysis showed that there was abundant $Be(OH)_2$ and $Be(NH_4)PO_4$ in the complexation products, which proved that surface complexation and precipitation reactions existed in the adsorption process.

4 Conclusions

A new, effective and inexpensive adsorption material modified porous lotus leaf biochar(MLLB) was successfully prepared. The introduction of phosphoric acid and ammonia was proved to effectively enhance the adsorption capacity Q_e of the biochar for Be. The adsorption thermodynamics and kinetics results indicated that adsorption equilibrium was reached within 2 h, and maximum adsorption efficiency of Be was 99%. According to adsorption isotherm fitting, the actual maximum saturated Q_e of MLLB for Be was 40.38 g kg^{-1} at 35 °C and pH=6, which is higher than most known adsorption materials. The beryllium separation coefficient by MLLB was $K_d=2.6\times10^4$ mL g^{-1}, which was much higher than other co-existing ions, indicating that MLLB owned high adsorption selectivity of Be towards ohter impurity ions. The characterization comparsion results of MLLB before and after adsorption indicated that there were abundant complexation products $Be(OH)_2$ and $Be(NH_4)PO_4$ on the surface of MLLB, proving that phosphate, ammonia, and hydroxyl groups would be complexed with beryllium. Then, it was inferred that surface complexation and precipitation reactions might co-existed during the adsorption process. To be concluded, the above findings were favorable to both the applicable use of agricultural waste and the alleviation of the environmental pressure caused by beryllium mining wastewater. The desorption beryllium solution would be used to prepare beryllium products after separation and purification, which would be further explored in subsequent researches.

Supplementary Information

The online version contains supplementary material available at https://doi.org/10.1007/s42773-024-00385-4.

Supplementary Material 1

Acknowledgements

We thank the following funding agencies for supporting this work: Research on characteristic properties of typical radioactive solid waste and radiation protection regulation technology and operation management mechanism (2019YFC1907701), The National Natural Science Foundation of China (52204363) and The Research Project of Hunan Provincial Education Department of China (No. 22B0440). The authors would like to express their gratitude to EditSprings (https://www.editsprings.cn) for the expert linguistic services provided. Test data provided by Luobo Lab (https://www.luobolab.com).

Author contributions

All authors contributed to the study conception and design. Material preparation, data collection and analysis were performed by Xu Zhao, Qingliang Wang, Boyuan Zheng, Yige Sun, Haoshuai Li, Zhiwu Lei, Hongyang Xia, Yucheng Su, Kham Muhammad Yaruq Ali, Fang Hu. The first draft of the manuscript was written by Xu Zhao and all authors commented on previous versions of the manuscript. All authors read and approved the final manuscript. Xu Zhao: Data curation, Writing. Boyuan Zheng: Data curation. Qingliang Wang: Funding acquisition. Yige Sun:Formal analysis. Haoshuai Li: Data curation. Zhiwu Lei: Data curation. Hongyang Xia: Data curation. Yucheng Su: Resources. Kham Muhammad Yaruq Ali: Data curation. Fang Hu: writing. Hongqiang Wang: Data curation.

Funding

Foundation of Ministry of Science and Technology of China, 2019YFC1907701, Research Project of Hunan Provincial Education Department of China, 22B0440, The National Natural Science Foundation of China,52204363.

Availability of data and materials

All data generated or analysed during this study are included in this published article (and its supplementary information files).

Declarations

Consent for publication

Not applicable.

Competing interests

The authors declare that they have no conflict of interest.

Author details

[1]School of Nuclear Science and Technology, University of South China, Hengyang 421001, Hunan, China. [2]School of Resource Environment and Safety Engineering, University of South China, Hengyang 421001, Hunan, China. [3]College of Resources and Environment, Anhui Agricultural University, Hefei 230000, Anhui, China. [4]School of Chemistry and Chemical Engineering, University of South China, Hengyang 421001, China.

Received: 15 April 2024 Revised: 30 August 2024 Accepted: 4 September 2024
Published online: 18 October 2024

References

Abd El-Magied MO, Mansour A, Al Ghani AIsayed FA, Eldayem SA (2018) Biosorption of beryllium from aqueous solutions onto modified chitosan resin: equilibrium, kinetic and thermodynamic study. J Dispers Sci Technol. https://doi.org/10.1080/01932691.2018.1452757

Al Isawi WA, Zeller M, Mezei G (2022) Supramolecular Incarceration and Extraction of Tetrafluoroberyllate from Water by Nanojars. Inorg Chem 61(23):8611–8622

Basargin NN, Miroshnichenko OV (2012) Beryllium (II) sorption from aqueous solutions by polystyrene–based chelating polymer sorbents. Russ J Inorg Chem 57(5):758–762

Bonilla-Petriciolet A, Mendoza-Castillo DI, Reynel-Ávila HE (eds) (2017) Adsorption processes for water treatment and purification. Springer, Cham, p 256

Bu X, Gier TE, Stucky GD (1998) Hydrothermal synthesis and low temperature crystal structure of an ammonium beryllophosphate with the merlinoite topology. Microporous Mesoporous Mater 26(1–3):61–66

Creutzenberg O, Hammann V, Wolf S, Daul J, Ngiewih Y, Chaudhuri I, Levy L (2022) Toxicokinetic study following intratracheal instillation or oral gavage of two [7Be]–tagged carbon black samples. Part Fibre Toxicol 19(1):63

De Sousa A (1975) Indirect complexometric determination of beryllium. Talanta 22(10–11):910–911

Desjardins SM, Ter-Mikaelian MT, Chen J (2024) Cradle–to–gate life cycle analysis of slow pyrolysis biochar from forest harvest residues in Ontario, Canada. Biochar 6(1):58

Fan Y, Song H, Wang Z, Gan N, Zhang C, Zhao B, Tan Y (2024) The behavior of pyrite during in–situ leaching of uranium by CO^2+ O^2: A case study of the Qianjiadian uranium deposit in the Songliao Basin, northeastern China. Ore Geol Rev:106085

Guerrero-Fajardo CA, Giraldo L, Moreno-Piraján JC (2020) Preparation and characterization of graphene oxide for Pb (II) and Zn (II) ions adsorption from aqueous solution: experimental, thermodynamic and kinetic study. Nanomaterials 10(6):1022

Islam MR, Sanderson P, Payne TE, Deb AK, Naidu R (2022) Role of beryllium in the environment: Insights from specific sorption and precipitation studies under different conditions. Sci Total Environ 838:155698

Jamil M, Elouahli A, Khallok H, Hatim Z (2019) Characterization of β–tricalcium phosphate–clay mineral composite obtained by sintering powder of apatitic calcium phosphate and montmorillonite. Surf Interfaces 17:100380

Krishnamoorthy KR, Iyer RK (1969) Homogeneous precipitation of beryllium by means of trichloroacetic acid hydrolysis and determination as phosphate. Anal Chim Acta 47(2):333–338

Labgairi K, Borji A, Kaddami M, Jourani A (2020) Kinetic study of calcium phosphate precipitation in the system H_3PO_4–Ca (OH) $_2$–H_2O at 30° C. Int J Chem Eng 2020:1–9

Laohavisuti N, Boonchom B, Boonmee W, Chaiseeda K, Seesanong S (2021) Simple recycling of biowaste eggshells to various calcium phosphates for specific industries. Sci Rep 11(1):15143

Lederer GW, Foley NK, Jaskula BW, Ayuso RA (2016) Beryllium—A critical mineral commodity—Resources, production, and supply chain (No. 2016–3081). US Geological Survey

Liu Y, Liu YJ (2008) Biosorption isotherms, kinetics and thermodynamics. Sep Purif Technol 61(3):229–242

Liu W, Zhang J, Zhang C, Wang Y, Li Y (2010) Adsorptive removal of Cr (VI) by Fe–modified activated carbon prepared from Trapa natans husk. Chem Eng J 162(2):677–684

Martins AC, Pezoti O, Cazetta AL, Bedin KC, Yamazaki DA, Bandoch GF, Almeida VC (2015) Removal of tetracycline by NaOH–activated carbon produced from macadamia nut shells: kinetic and equilibrium studies. Chem Eng J 260:291–299

Mirzaeei S, Pirhayati FH, Mohammadi G, Rahimpour E, Martinez F, Jouyban A (2019) Solubility of minoxidil in binary mixture of ethanol+ water at various temperatures. Phys Chem Liq 57(6):788–799

Petidier A, Rubio S, Gomez-Hens A, Valcarcel M (1985) Fluorimetric determination of beryllium with pyridoxal–5–phosphate. Talanta 32(11):1041–1045

Pezoti O, Cazetta AL, Bedin KC, Souza LS, Martins AC, Silva TL, Almeida VC (2016) NaOH–activated carbon of high surface area produced from guava seeds as a high–efficiency adsorbent for amoxicillin removal: Kinetic, isotherm and thermodynamic studies. Chem Eng J 288:778–788

Polowczyk I, Bastrzyk A, Fiedot M (2016) Protein–mediated precipitation of calcium carbonate. Materials 9(11):944

Puettmann M, Sahoo K, Wilson K, Oneil E (2020) Life cycle assessment of biochar produced from forest residues using portable systems. J Clean Prod 250:119564. https://doi.org/10.1016/j.jclepro.2019.119564

Qu J, Li Z, Bi F, Zhang X, Zhang B, Li K, Zhang Y (2023) A multiple Kirkendall strategy for converting nanosized zero–valent iron to highly active Fenton–like catalyst for organics degradation. Proc Natl Acad Sci 120(39):e2304552120

Qu J, Li Y, Sun H, Liu R, Han Y, Bi F, Zhang Y (2024) Ball–milled sepiolite/phosphate rock for simultaneous remediation of cadmium–contaminated farmland and alleviation of phosphorus deficiency symptoms in pepper. Chem Eng J 488:150925

Ren Z, Jia B, Zhang G, Fu X, Wang Z, Wang P, Lv L (2021) Study on adsorption of ammonia nitrogen by iron–loaded activated carbon from low temperature wastewater. Chemosphere 262:127895

Senthil Kumar P, Dinesh Kirupha S et al (2011) Adsorption behavior of nickel(II) onto cashew nut shell: Equilibrium, thermodynamics, kinetics, mechanism and process design(J). Chem Eng J 167:122–131

Shchukarev AV, Korolkov DV (2004) XPS study of group IA carbonates. Cent Eur J Chem 2(2):347–362

Sternik D, Gładysz-Płaska A, Grabias E, Majdan M, Knauer W (2017) A thermal, sorptive and spectral study of HDTMA–bentonite loaded with uranyl phosphate. J Therm Anal Calorim 129:1277–1289

Sun F, Sun WL et al (2011) Biosorption behavior and mechanism of beryllium from aqueous solution by aerobic granule(J). Chem Eng J 172(2–3):783–791

Tanveer M, Wang L (2019) Potential targets to reduce beryllium toxicity in plants: a review. Plant Physiol Biochem 139:691–696

Thommes M, Kaneko K, Neimark AV, Olivier JP, Rodriguez-Reinoso F, Rouquerol J, Sing KS (2015) Physisorption of gases, with special reference to the evaluation of surface area and pore size distribution (IUPAC Technical Report). Pure Appl Chem 87(9–10):1051–1069

Tokarčíková M, Motyka O, Peikertová P, Gabor R, Seidlerová J (2021) Magnetically modified biosorbent for rapid beryllium elimination from the aqueous environment. Materials 14(21):6610

Touny AH, Saleh MM (2018) Fabrication of biphasic calcium phosphates nanowhiskers by reflux approach. Ceram Int 44(14):16543–16547

Wei X, Huang S, Wu Y, Wu S (2022) Effects of demineralization and devolatilization on fast pyrolysis behaviors and product characteristics of penicillin mycelial residues. J Hazard Mater 430:128359

Wu FC, Tseng RL, Juang RS (2005) Comparisons of porous and adsorption properties of carbons activated by steam and KOH. J Colloid Interface Sci 28:49–56

Xin Q, Wang Q, Gan J, Lei Z, Hu E, Wang H, Wang H (2023) Enhanced performance in uranium extraction by the synergistic effect of functional groups on chitosan–based adsorbent. Carbohyd Polym 300:120270

Zhang X, Li Y, Wu M, Pang Y, Hao Z, Hu M, Chen Z (2021) Enhanced adsorption of tetracycline by an iron and manganese oxides loaded biochar: Kinetics, mechanism and column adsorption. Biores Technol 320:124264

Zhao X, Su Y, Lei Z, Wang H, Hu E, Hu F, Hao X (2023a) Adsorptive removal of beryllium by Fe–modified activated carbon prepared from lotus leaf. Environ Sci Pollut Res 30(7):18340–18353

Zhao X, Dong S, Wang H, Hu E, Hu F, Lei Z, Su Y (2023b) Preparation of porous calcium carbonate biochar and its beryllium adsorption performance. J Environ Chem Eng 11(3):110102

Zhao X, Wang Q, Sun Y, Li H, Lei Z, Zheng B, Hu F (2024) An eco–friendly porous hydrogel adsorbent based on dextran/phosphate/amino for efficient removal of Be (II) from aqueous solution. Int J Biol Macromol 269:131851

Zhao X, Su Y, Hao X, Wang H, Hu E, Hu F, Dong S (2023c) Effect of mechanical–chemical modification on adsorption of beryllium by calcite. Environ Sci Pollut Res:1–13

Zheng Y, Wang Z, Liu C, Tao L, Huang Y, Zheng Z (2020) Integrated production of aromatic amines, aromatic hydrocarbon and N–heterocyclic bio–char

from catalytic pyrolysis of biomass impregnated with ammonia sources over Zn/HZSM−5 catalyst. J Energy Inst 93(1):210–223
Zhong S, Hu M, Zhang L, Qin X, Zhang Q, Ru X (2023) Toxic metals and the risks of sludge from the treatment of wastewater from beryllium smelting. Chemosphere 326:138439